Biomaterials Science

ROYAL SOCIETY OF CHEMISTRY

PAPER

View Article Online
View Journal | View Issue

Check for updates

Cite this: *Biomater. Sci.*, 2023, **11**, 3114

Nitric oxide-releasing poly(ionic liquid)-based microneedle for subcutaneous fungal infection treatment†

Qiuyang Zhang, Zijun Zhang, Xiuyang Zou, Ziyang Liu, Qingning Li, Jiamei Zhou, Shuna Gao, Hui Xu, Jiangna Guo * and Feng Yan *

Received 20th December 2022,
Accepted 2nd March 2023

DOI: 10.1039/d2bm02096c

rsc.li/biomaterials-science

Poor permeation of therapeutic agents and similar eukaryotic cell metabolic and physiological properties of fungi and human cells are two major challenges that lead to the failure of current therapy for fungi-induced skin and soft tissue infections. Herein, a nitric oxide (NO)-releasing poly(ionic liquid)-based microneedle (PILMN-NO) with the capacity of deep persistent NO toward subcutaneous fungal bed is presented as a synergistic antifungal treatment strategy to treat subcutaneous fungal infection. Upon the insertion of PILMN-NO into skin, the contact fungicidal activities induced by electrostatic and hydrophobic effects of poly(ionic liquid) and the released NO sterilization resulting from the peroxidation and nitrification effect of NO achieved enhanced antifungal efficacy against fungi (*Candida albicans*) both *in vitro* and *in vivo*. Simultaneously, PILMN-NO showed biofilm ablation ability and efficiently eliminated mature biofilms. *In vivo* fungal-induced subcutaneous abscess studies revealed that PILMN-NO could effectively sterilize fungi while suppressing the inflammatory reaction, facilitating collagen deposition and angiogenesis, and promoting wound healing. This work provides a new strategy to overcome the difficulties in deep skin fungal infection treatment and has potential for further exploitation of NO-releasing microbicidal therapy.

Published on 07 martie 2023. Downloaded on 05.06.2026 15:08:56.

1. Introduction

Skin and soft tissue infections (SSTIs), especially those caused by fungi, are extremely stubborn and affect global health.[1–3] Candida species-induced SSTIs are difficult to eliminate due to the similar eukaryotic cell properties of fungi and human cells, and host and geographic factors complicate antifungal therapy.[4,5] Candida species, particularly *C. albicans*, may cause skin and soft tissue infections and induce superficial or invasive diseases, such as chronic mucocutaneous candidiasis, central nervous system (CNS) candidiasis and mucocutaneous candidiasis.[6] Fungi-induced skin infections are currently treated with antifungal-containing topical creams, ointments, gels, or lotions and oral administration of antifungal agents. Oral drugs show low bioavailability and cannot target the site of infection simultaneously. Topical antifungal cream applications may efficiently treat superficial infections but fail to eliminate deep cutaneous infections since the drug cannot effectively penetrate through the stratum corneum. Moreover, topical antifungal creams need to be used multiple times during fungal infection treatment.[7] Furthermore, the stratum corneum layer of the skin, an important drug transport barrier, may obstruct antifungal treatment, leading to a traditional treatment time for fungal infections of up to several months.[8] Meanwhile, proliferating fungi are prone to form subcutaneous biofilms, causing severe inflammation and abscesses.[9] Moreover, traditional antifungal agents promote the emergence of resistant fungi, further challenging the treatment of such infections.[10] To confront these problems, an innovative and efficient antifungal strategy is urgently needed and highly desirable.[11]

Endogenic nitric oxide (NO), a lipophilic free radical diffusible gaseous molecule that participates in multiple physiological processes, can be produced by endothelial (eNOS), neuronal (nNOS), and inducible (iNOS) cells in the presence of L-arginine.[12] Recently, NO, as an attractive alternative to traditional antibiotics without displaying drug resistance for microbial infections, has been extensively explored as an anti-

Jiangsu Engineering Laboratory of Novel Functional Polymeric Materials, Jiangsu Key Laboratory of Advanced Negative Carbon Technologies College of Chemistry, Suzhou Key Laboratory of Soft Material and New Energy, College of Chemistry, Chemical Engineering and Materials Science, Soochow University, Suzhou, 215123, China. E-mail: guojn@suda.edu.cn, fyan@suda.edu.cn

†Electronic supplementary information (ESI) available: Experimental section, photographs and optical microscope of pinholes after insertion of PILMN-NO, calibration curve of NO, the colony plate photographs and TEM images of *C. albicans*, fluorescence images of chitin and the colony plate photographs of *C. albicans in vivo*. See DOI: https://doi.org/10.1039/d2bm02096c

This journal is © The Royal Society of Chemistry 2023

Published on 07 martie 2023. Downloaded on 05.06.2026 15:08:56.

microbial agent.[13] NO shows broad-spectrum antimicrobial activities against bacteria and fungi and exerts biofilm inhibition and elimination properties both *in vitro* and *in vivo* due to its reactive byproducts (*e.g.*, peroxynitrite and dinitrogen trioxide), which can exert nitrosative or oxidative stress, disrupting the microbial membrane and compromising cell function, ultimately inducing microbial death.[14–17] Additionally, an appropriate dose of NO exerts a good anti-inflammatory effect and can promote infection elimination.[18,19] Moreover, NO can promote the production of collagen during tissue reconstruction and induce angiogenesis, accelerating wound healing.[20] Given these great merits, it is expected that NO represents a versatile antimicrobial agent for the effective treatment of subcutaneous abscesses. However, NO donors, such as organic nitrate, metal nitrosy and *S*-nitrosothiol, are challenging due to strict trigger conditions and high toxicity. For *N*-diazeniumdiolate, the preparation of which should be performed under hyperbaric and alkalic conditions.[21] Recent studies have shown that ionic liquids (ILs) can be used as good absorbents for NO capture and release at atmospheric pressure.[22] ILs with functional anions, such as anhydrous benzenesulfonic acid, trichloroacetic acid, and L-proline, can bind NO through chemical bonds to form a new NO donor, creating superhigh NO absorbing capacity and good reversibility without the abovementioned shortcomings.[23,24] Poly(ionic liquid)s (PILs) with various properties of small molecule ILs and polymers show unique advantages, overcoming the application limitations of small molecule bactericidal ILs.[25–29] Additionally, the clinical application of NO is limited by the lack of localized delivery. Therefore, the development of a multifunctional NO delivery system based on PILs could be a more practical approach for the treatment of subcutaneously infected abscesses.[30]

Microneedles (MNs) as a precise delivery system has attracted significant attention in recent years.[31] MN with adjustable needle length (50–900 μm) can create transient pores in the outermost layer of the epidermis painlessly and are widely utilized in biomedical applications, such as drug delivery, biosensing and therapeutic diagnoses.[32–35] Various materials, such as metals and polymers, have been used to prepare MNs.[36,37] MNs have been used for the treatment of microbial or biofilm infection by delivering antimicrobial compounds, such as antibiotics, antibacterial peptides, and carbon-based materials, into the skin to inhibit and kill microbes.[38–40] In general, the antimicrobial agents are encapsulated in the needles of MNs that are inserted into skin tissue to release the encapsulated antimicrobial agents in the deep layer of the dermis to kill microbes.[41] Although MN patches offer apparent advantages in the transdermal delivery of antimicrobial agents, most reported MNs patches lack intrinsic antimicrobial abilities and may induce infection at the insertion site.[42] Therefore, the construction of MNs with antimicrobial and anti-inflammatory activities and exploration of their application in subcutaneous microbial-induced infection treatments are important and significant.[7]

Here, for the first time, a simplistic strategy of constructing NO-releasing imidazolium-type PIL-based MN patches (PILMN-NO) for the treatment of fungal-induced skin and soft tissue infection is reported. PILMN-NO patches were prepared by photocrosslinking 3-(2-hydroxyethyl)-1-vinylimidazolium 3-amino-1-propanesulfonic acid ([HEIm][APS]) and hydroxyethyl acrylate (HEA) with poly(ethylene glycol) diacrylate (PEGDA) as a crosslinker followed by absorption of NO by forming a hydrogen bond with APS^-. PILMN-NO can release NO under physiological conditions and exhibit potent synergistic antifungal action against fungi (*Candida albicans*), as well as biofilm ablation ability *in vitro* due to the cationic PILs and released NO. Coupled with good biocompatibility, the PILMN-NO shows effective fungicidal, anti-inflammatory, collagen deposition and angiogenesis activities in *Candida albicans*-induced subcutaneous abscess infection, promoting infection elimination and wound healing in an *in vivo* mouse model.

2. Results and discussion

Scheme 1 illustrates NO-releasing imidazolium-type PIL-based MN patches (PILMN-NO) enabling NO delivery for subcutaneous fungal infection treatment. PILMN-NO was prepared by photocrosslinking [HEIm][APS], HEA and PEGDA with HCPK as a photoinitiator in a PDMS mold under UV irradiation (365 nm, 30 min) followed by exposure to a NO atmosphere for 4 h for APS^- reacting with NO to form IL-*N*-diazeniumdiolates (IL-NONOates). NO is absorbed by the [HEIm][APS] section through a chemical reaction between the $-NH_2$ in the APS^- and NO (Scheme S1†). PILMN-NO was applied to treat a *C. albicans*-induced subcutaneous abscess infection mouse model and showed effective fungicidal, anti-inflammatory, collagen deposition, and angiogenesis activities *in vivo*, exerting infection elimination and wound healing activities.

Preparation and characterization of MNs

Different from traditional NONOates, PIL can absorb NO at atmospheric pressure to form NONOate groups. To better study the NONOate groups formed between PIL and NO, an imidazole-type PIL was first synthesized. As demonstrated in Fig. 1a, ^1H NMR spectroscopic analysis revealed a new peak at 8.79 ppm in PIL-NO, reflecting the formation of NONOates through intramolecular hydrogen bonds compared to PIL. Also, Fourier transform infrared spectroscopy (FT-IR) shows new peaks at 823 and 1335 cm^{-1} corresponding to ν(N–N), and peaks at 1259 and 1549 cm^{-1} for ν(N–O) appeared in PIL-NO, indicating the NO absorption of PIL by forming NONOates (Fig. 1b).[43] Fig. 1c shows the geometry optimization of the linear structure and hydrogen bond stabilized structure and the energy gap between them. The interatomic distance between the O on the sulfonyl carboxyl group and the H on the NONOate group is 1.623 Å, which is in the range of hydrogen bonding, confirming the formation of intramolecular hydrogen bonds between APS^- and the absorbed NO. Moreover, the energy level of [APS]-NONO decreases after the

Published on 07 martie 2023. Downloaded on 05.06.2026 15:08:56.

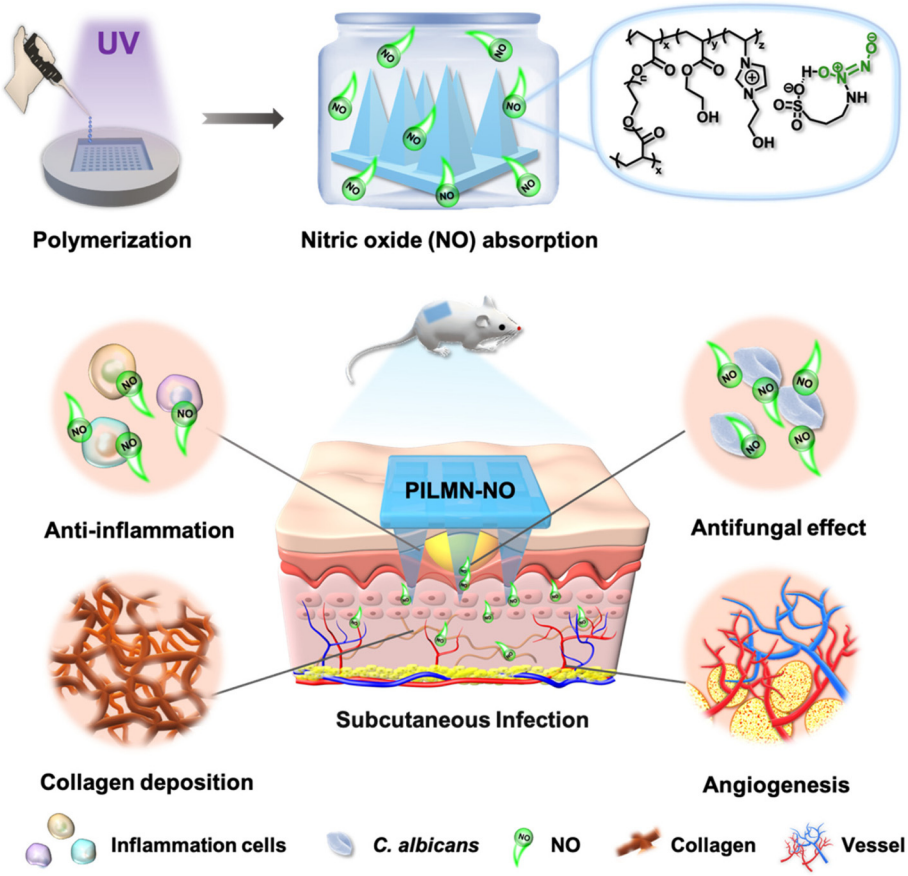

Scheme 1 Schematic illustrating the synthesis of NO-releasing imidazolium-type PIL-based microneedle patches (PILMN-NO) and corresponding fungi killing, anti-inflammation, collagen deposition and angiogenesis activities for promoting infection elimination and accelerating wound healing.

formation of intramolecular hydrogen bonds, indicating that the formed hydrogen bond stabilizes the structure. These results prove that PIL can combine NO by the formation of NONOate groups. PILMN was developed and kept under a saturated atmosphere of NO to prepare PILMN-NO. Similar FT-IR results were obtained in PILMN-NO, suggesting the combination of PILMN and NO by forming NONOate groups. Four new peaks appeared at 823, 1259, 1341 and 1552 cm^{-1} (Fig. 1b), revealing that PILMN is capable of absorbing NO, confirming the synthesis of NO-adsorbed MNs. Additionally, the predicted chemical shift of the hydrogen bond by quantum chemical calculations is 11.05 ppm, and the predicted peaks of ν(N–N) and ν(N–O) are located at 836, 1259, 1335 and 1526 cm^{-1}, which are close to the experimental results, as shown in Fig. 1c. All the above results indicate that NO has combined with the APS^{-} in PIL by the formation of NONOate groups.

The macroscopic and microscopic images of PILMN are shown in Fig. 1d, which suggest that the PILMN possesses a regular array arrangement with sharp needles, and the needles are quadrangular pyramids with complete tips, approximately 720 μm in height, 320 μm in diameter at the base, and 680 μm between tips. In addition, the morphology of MN patches does not change after NO absorption (Fig. 1e), indicating the stability of PILMN and PILMN-NO. After insertion into the isolated fresh rabbit cadaver skin, the tips of the MNs are slightly frayed and bent, and the surface becomes rougher (Fig. 1f). All these results confirm the successful preparation and perfectly organized appearance of PILMN-NO.

Mechanical properties and NO release of MNs

High mechanical strength of MNs is necessary as wound patches. According to the rheological test, the G' and G'' of the gels on frequency sweep from 0.1 to 10 can be seen in Fig. 2a. Compared with PILMN, the G' and G'' of PILMN-NO slightly decreased because of the introduction of NO. The mechanical properties of MN patches were further measured (Fig. 2b). The mechanical strength of the cross-linked PILMN and PILMN-NO is similar with compression stress of approximately 2.0 and 1.7 MPa, with a compression strain of 50% and elastic behavior without residual strain. Fig. 2c shows the force-displacement curves of PILMN and PILMN-NO recorded within 600 μm. As the displacement increases to 400 μm, the force for PILMN and PILMN-NO gradually increases to approximately 10 N, indicating that both PILMN and PILMN-NO possess enough

 This journal is © The Royal Society of Chemistry 2023

Published on 07 martie 2023. Downloaded on 05.06.2026 15:08:56.

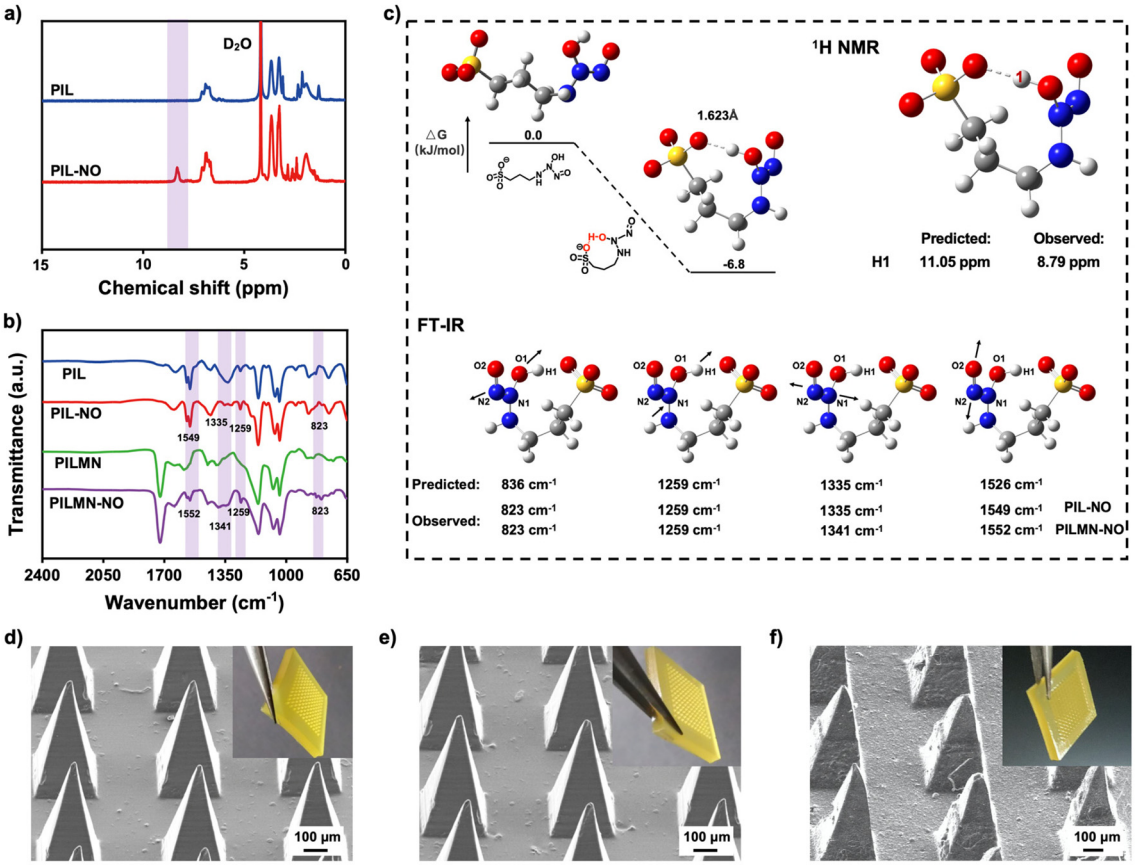

Fig. 1 Chemical structure characterization and morphology images of MNs. (a) ^{1}H NMR spectra of PIL and PIL-NO. (b) FT-IR spectra of PIL, PIL-NO, PILMN and PILMN-NO. (c) Energy gap between two different structures of [APS]-NONO. Prediction of the FT-IR vibration model and ^{1}H NMR spectra for [APS]-NONO. SEM images of the freshly prepared (d) PILMN, (e) PILMN-NO and (f) PILMN-NO after insertion into the isolated skin (insert: corresponding images).

mechanical strength to penetrate skin.[44] The stability of PILMN-NO was further studied after storing in NO atmosphere for 2 days. As shown in Fig. S1,† the force for PILMN-NO gradually increases to approximately 15 N, indicating the mechanical stability of PILMN-NO. *In vitro* and *in vivo* skin insertion ability was further confirmed by inserting PILMN-NO patches into the isolated fresh rabbit cadaver skin and live mice with approximately 8 N pressure for 1 min, respectively. The pinholes created by PILMN-NO are clearly visible (Fig. S2†). Fungal infection usually occurs in the dermis of the skin, which is generally located about 200 μm below the skin. As is shown in Fig. S3,† the length of the visible pinhole remaining in the skin is 260 μm, indicating that the length of the PILMN-NO is long enough to penetrate the dermis. All these results indicate that the good mechanical properties of MN are suitable for skin penetration at an adequate depth.

NO is absorbed by PILMN through intramolecular hydrogen bonds between anionic APS^- and NO, which can be released at physiological temperature and pH. PILMN-NO could be easily prepared by bubbling NO into PILMN to form NONOate groups in a confined and oxygen-free system. NO absorption was investigated through gravimetric method, and the result suggests that the NO absorption capacity of PILMN is 1.26 mol NO per mol PIL for 4 h (Fig. 2d), and the [APS]-NONO in PILMN-NO is calculated to be 2.31 wt%. Griess assay was used to quantitatively analyze NO release from PILMN-NO both *in vivo* and *ex vivo*. PILMN-NO was immersed in a PBS solution, and the absorbance of the supernatant was monitored over time by UV-vis spectroscopy (540 nm). As illustrated in Fig. 2e–h, both *in vitro* and *ex vitro*, a sustained release of NO is observed, which can last approximately 80 min. NO releases quickly in the initial 10 min and then gradually slows down. The NO concentration increased with time, reaching a maximum of 510 μM *in vitro* according to the standard curve (Fig. S4†) at 80 min, while at 10 min, 470 μM NO was released, which was 92.1% of the maximum value. An *ex vitro* NO release test was performed using a transdermal diffusion apparatus. Similar results were obtained in the *ex vivo* release assay with a maximum release amount of 12 μM, and the initial release in the first 10 min was 9 μM. These results suggest that the released NO amount is capable of eliminating fungi since 10^{-6}–10^{-3} M NO can effectively kill fungi but exhibits no significant toxicity against mammalian cells.[21]

Published on 07 martie 2023. Downloaded on 05.06.2026 15:08:56.

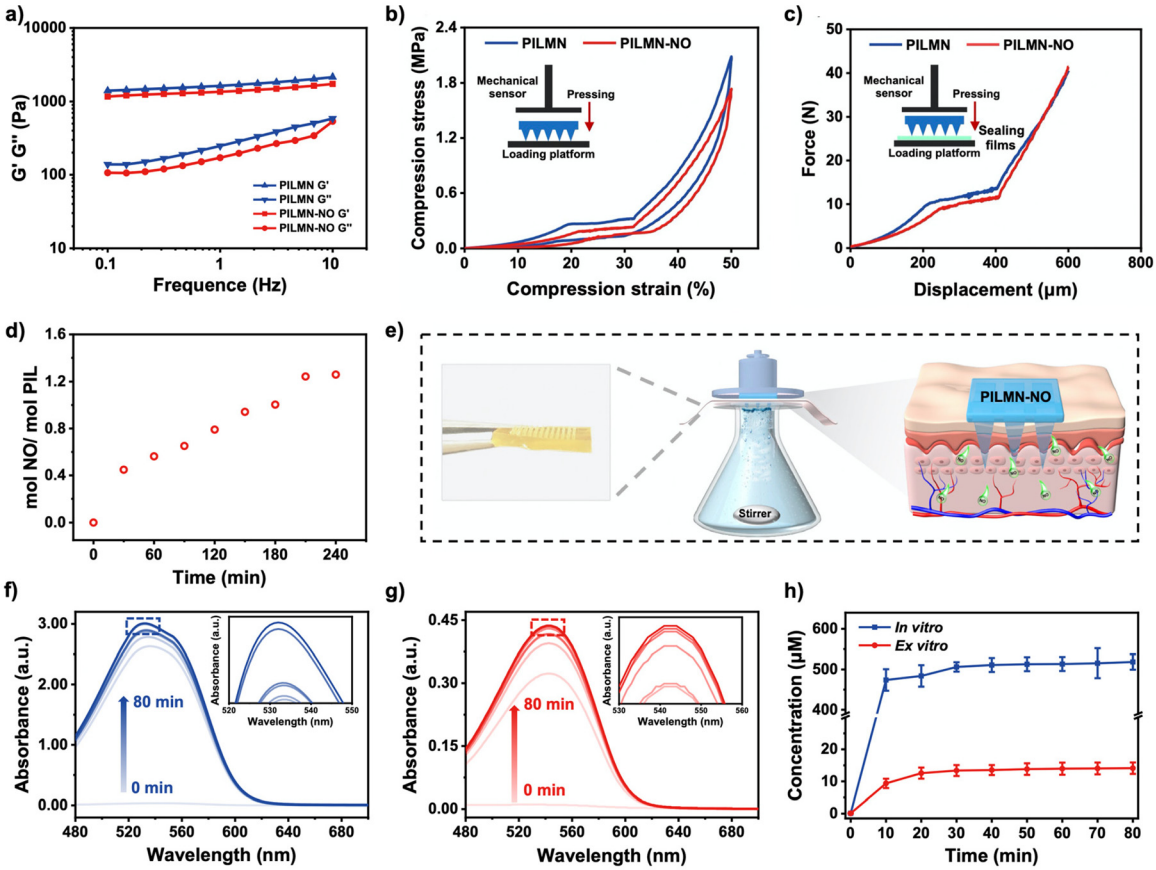

Fig. 2 Mechanical properties and NO release of MNs. (a) Storage and loss moduli of MN patches at different frequencies. (b) Compression stress–strain of PILMN and PILMN-NO. Hysteresis loops under 50% compression strain. (c) Force-displacement curves of PILMN and PILMN-NO recorded during penetrating eight-layer sealing films at 400 μm. (d) NO absorption curve by PILMN at 25 °C and 1 bar. (e) Schematic illustration of the *ex vivo* study of NO release from PILMN-NO and transdermal diffusion. (f) UV-vis spectra monitoring of *in vitro* NO release from PILMN-NO at pH 7.4 and 37 °C. (g) UV-vis spectra monitoring of *ex vitro* NO release from PILMN-NO at pH 7.4 and 37 °C. (h) Real-time NO release profile of PILMN-NO in PBS (pH = 7.4) from t = 0 min to t = 80 min at 37 °C *in vitro* and *ex vivo*. Error bars are based on SD (n = 3).

In vitro antifungal activity and biofilm elimination effect

SSTIs caused by fungi are one of the main causes of subcutaneous inflammation. The cell structure of fungi is more complex than that of bacteria, which makes the treatment of fungal infection more challenging. Here, *C. albicans* was used as a fungal model to evaluate the antifungal activity of the synthesized MNs. As shown in Fig. 3a and Fig. S5,† PILMN can inhibit the proliferation of *C. albicans*, and 19.03% ± 2.25% of *C. albicans* remained viable, while PILMN-NO completely inactivated *C. albicans*, suggesting its efficient fungicidal activity. Additionally, the fungal viability increased with the concentration of PIL decreased. As shown in Fig. S6 and S7,† the antibacterial rate of $PILMN_{10}$-NO and $PILMN_{20}$-NO was 95.62% and 99.43%, respectively. PILMN killed *C. albicans* due to the fungicidal properties of PIL sections, which may destroy the cellular structure of fungi, such as leakage of intracellular materials, a decrease in ergosterol, and damage to mitochondria.[45] However, the potent fungicidal property of PILMN-NO can be explained by the synergistic effect of the PIL section and the released NO. The released NO from PILMN-NO may destroy fungal structures by lipid peroxidation, membrane nitrification, and damage from active nitrogen byproducts, such as nitrous oxide.[46] Additionally, the released NO from PILMN-NO induces a noticeable inhibition zone against *C. albicans* (Fig. 3b) compared to PILMN, suggesting the fungicidal performance of NO. Live/dead microbial staining images further confirm the fungicidal activity of PILMN and PILMN-NO (Fig. 3c). *C. albicans* in the control group emitted bright green fluorescence, indicating fungal viability. In contrast, fungi treated with PILMN scattered red fluorescence with some green fluorescence, suggesting the death of most fungi. Only red fluorescent signals of dead fungi were observed in the PILMN-NO-treated group, demonstrating a good sterilization effect of PILMN-NO due to the synergetic effect of NO and PILs. Fig. 3d shows the microscopic changes in *C. albicans* after treatment with the synthesized MNs. Compared with the live fungi with spherical and smooth surfaces in the control group, dead fungi showed a flat shape with a collapsed cell surface in the PILMN treated group, and more severe cell col-

 This journal is © The Royal Society of Chemistry 2023

Published on 07 martie 2023. Downloaded on 05.06.2026 15:08:56.

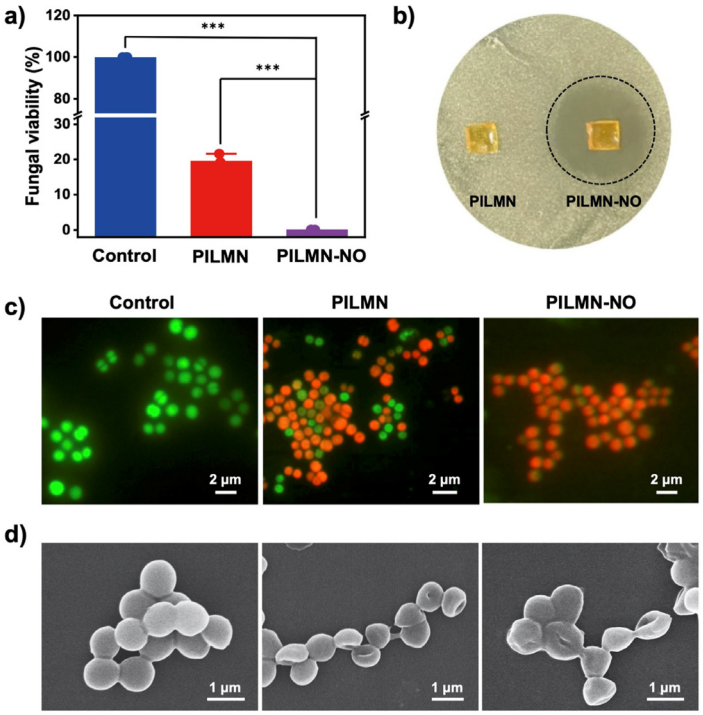

Fig. 3 *In vitro* antifungal activity of the synthesized MNs. (a) *C. albicans* viabilities after being treated with PILMN and PILMN-NO for 2 h. Error bars are based on SD (n = 3). Note: *p < 0.05, **p < 0.01, and ***p < 0.001. (b) Images of inhibition zones of PILMN and PILMN-NO towards *C. albicans*, respectively. (c) Live/dead staining images and (d) SEM images of *C. albicans* treated with PILMN and PILMN-NO.

lapse and wrinkles were observed in the PILMN-NO-treated group due to cytoplasm leakage. Similar results were obtained by TEM, which revealed a clear intact structure and smooth cell walls in the control group of *C. albicans*, while damaged and blurred cell walls were observed in PILMN-treated groups (Fig. S8†). For the PILMN-NO-treated fungi, the cell walls were severely broken with incomplete cell structures. These results indicate that the dead fungi induced by the synthesized MNs present significant cell membrane destruction. The fluorescent staining, SEM and TEM images validate that the antifungal properties of PILMN and PILMN-NO may derive from a membrane destruction sterilization mechanism.

Biofilms are composed of microbial cell clusters encased in extracellular polymeric substances (EPSs).[47] Approximately 80% of microbial infections are biofilm-associated, since biofilms may form in acute and chronic wounds, impeding the healing process. Compared with microbes, biofilms may inhibit drug penetration, limit nutrition supply, and slow bacterial growth while decreasing microbial susceptibility to antibiotics. Inhibiting/eliminating biofilms is a serious challenge and research hotspot. Encouraged by the superior antifungal effect of PILMN and PILMN-NO, the biofilm elimination effect of the synthesized MNs was further examined. The biofilm mass with different treatments was evaluated by crystal violet staining assay. As shown in Fig. 4a, compared to biofilm without any treatment, the remaining biofilm mass after treatment with PILMN was 32.91% ± 1.49%, while only 16.27% ± 1.38% biofilm mass was residual after treatment with PILMN-NO, suggesting an efficient biofilm elimination effect of NO. In the presence of NO (10^{-6}–10^{-3} M), the EPS matrix may be altered, causing biofilm physical destruction by inducing oxidative damage to the intercellular matrix, reducing the interaction between fungi as well as the binding force between fungi and matrix, resulting in disruption and detachment in biofilms.[48] Furthermore, spectroscopic observation of fungi detached from the biofilm at 490 nm (Fig. 4b) reveals that the prepared MNs can dissociate the biofilms more completely and release more fungi.[49] To better evaluate the biofilm elimination ability of PILMN-NO, a live/dead staining assay was performed for CLSM. The biofilms in the control group emitted strong green fluorescence, while the biofilm treated with PILMNs scattered red fluorescence, verifying the fungicidal activities of PILMN within biofilms (Fig. 4c). Notably, stronger red fluorescence is observed after treatment with PILMN-NO, suggesting superior fungicidal and biofilm destruction properties of PILMN-NO. The fungi within the biofilms are killed by NO released from PILMN-NO during oxidative damage to the intercellular matrix of the biofilm.[50] The fluorescence intensity of the red signal was further quantified with ImageJ (Fig. 4d), showing a decrease in fluorescence intensity as follows: control > PILMN > PILMN-NO, demonstrating a gradual increase in biofilm destruction and fungal death. These results further confirm the synergy of PIL and NO

Published on 07 martie 2023. Downloaded on 05.06.2026 15:08:56.

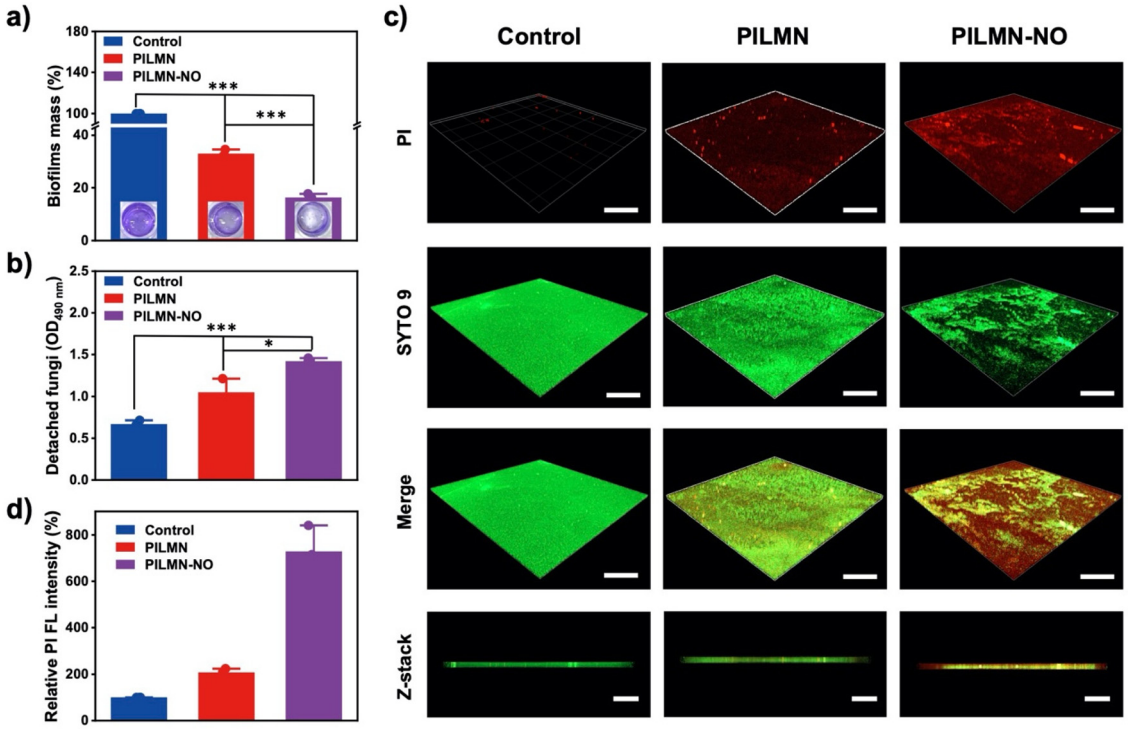

Fig. 4 *In vitro* biofilm ablation effect of the synthesized MNs. (a) Biofilm mass after treatment with PILMN and PILMN-NO (insert: photographs of the remaining *C. albicans* biofilms stained with crystal violet). Error bars are based on SD (n = 3). Note: *p < 0.05, **p < 0.01, and ***p < 0.001. (b) Absorbance of detached fungi released from mature biofilms at a wavelength of 490 nm. Error bars are based on SD (n = 3). Note: *p < 0.05, **p < 0.01, and ***p < 0.001. (c) CLSM images of *C. albicans* biofilms after treatment with PILMN and PILMN-NO (scale bar: 200 μm). (d) Fluorescence intensity of the red fluorescence emitted from *C. albicans* analyzed by ImageJ.

for biofilm elimination, highlighting the importance of the released NO.

Antifungal mechanism of the synthesized MNs

Imidazolium-based PILMN is considered to achieve fungicidal activity *via* a cell membrane destruction mechanism.[51] In the case of PILMN-NO, in addition to membrane damage caused by the electrostatic and hydrophobic effects of PIL, the released NO exerts fungicidal action by damaging fungal cell membrane components by reacting to form reactive nitrogen species (RNS), which are all catastrophic cytotoxic events for microbes.[52] To reveal the antifungal mechanism of PILMN and PILMN-NO, membrane solidarity was first characterized using *C. albicans* as a fungal model. Fungal cell walls are composed of chitin in the inner layer and glucan and mannan in the outer layer.[53] Accordingly, a β-glucanase sensitivity assay and chitin estimation were performed to reveal the effect of the synthesized MNs on the fungal cell wall. Spectroscopic monitoring for 200 min depicted the varied cell lysis activity of *C. albicans* with different treatments (Fig. 5a). After 200 min of incubation, the absorbance of *C. albicans* decreased to nearly 73%, 68% and 63% in the control, PILMN, and PILMN-NO treated groups, respectively, suggesting varied activities of the β-1,3-glucanase enzyme after different treatments. Therefore, PILMN-NO significantly potentiates enzyme activity by interacting with β-glucan, increasing the fragility of fungal cell walls and facilitating cell lysis. Chitin quantification was performed by staining *C. albicans* with CFW 28, and the variation in fluorescent intensity was used to evaluate the change in chitin content (Fig. S9†). The blue fluorescence intensity of *C. albicans* was as follows: control > PILMN > PILMN-NO, and the chitin presented in the *C. albicans* cell wall showed a significant reduction after treatment with PILMN-NO, suggesting the destruction of the fungal cell wall. Moreover, the fluorescence spectra display a similar change, demonstrating a decrease in chitin after treatment with PILMN and PILMN-NO (Fig. 5b). These findings indicate that chitin is an important target for PIL and NO to force fungal cell wall disruption. Overall, PILMN-NO may perturb fungal cell wall stability by interacting with cell wall components. Next, the membrane fluidity and esterase activity of *C. albicans* treated with the synthesized MNs were further measured. DPH, which fluoresces upon intercalation with lipids, was used to study membrane fluidity. Fig. 5c shows a significant increase in the fluorescence intensity of *C. albicans* after PILMN and PILMN-NO treatment, especially in PILMN-NO-treated cells, compared to the control group. The enhancement in fluorescence intensity suggests an increase in membrane fluidity, reflecting the interaction of PIL and NO with the plasma membrane. Additionally, the membrane disruption accrued during the fungicidal activity can be further proven by evaluating the fluorescence of cFDA-SE, which can permeate microbial cell walls/membranes after

 This journal is © The Royal Society of Chemistry 2023

Published on 07 martie 2023. Downloaded on 05.06.2026 15:08:56.

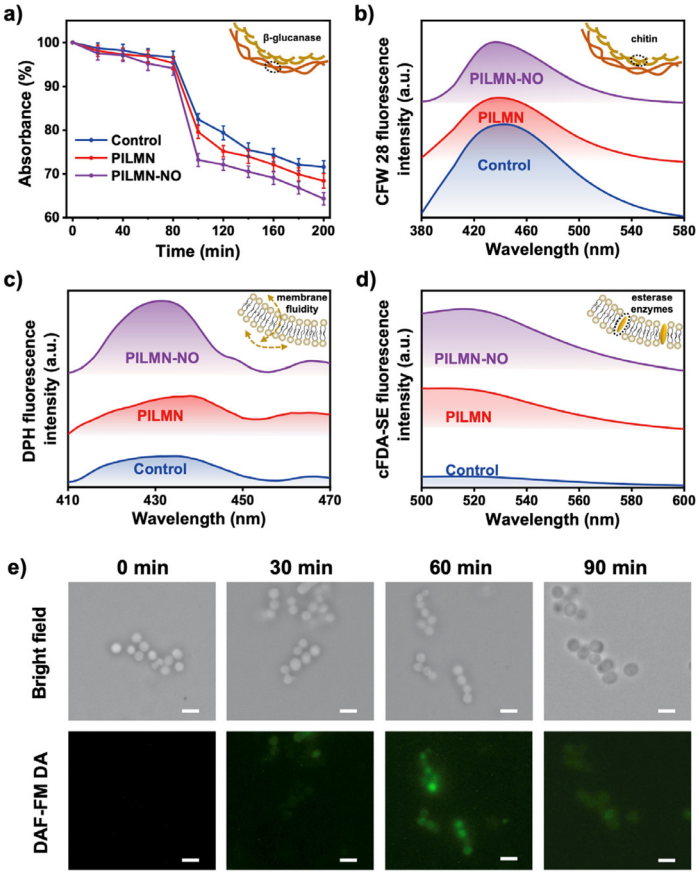

Fig. 5 (a) Spectroscopic estimation of β-1,3-glucan in *C. albicans* cells using β-glucanase. Optical density: 600 nm (insert: cell walls containing β-1,3-glucan). (b) Estimation of chitin with fluorescence spectra by evaluating the fluorescence density of calcofluor white 28-stained *C. albicans* cells (insert: cell walls containing chitin). (c) Spectroscopic analysis of membrane fluidity by measuring the DPH intensity in *C. albicans* cells (insert: cell membrane fluidity). (d) cFDA-SE leakage assay on target cells of *C. albicans* under different treatments (insert: cell membranes containing esterase enzymes). (e) Visible fluorescence images for real-time detection of NO in *C. albicans* (scale bar: 2 μm).

esterase hydrolysis and emit fluorescence at 518 nm. As shown in Fig. 5d, the very weak fluorescence intensity in the control group indicates the integrity of fungal membranes. However, after treatment with PILMN, the fluorescence intensity increased, which validates the disruption of the fungal membrane. Stronger fluorescence was detected in the PILMN-NO-treated group due to the synergistic effect of PIL and released NO, suggesting more severe membrane damage. Overall, all the above results establish that PILMN-NO targets membrane permeability and destroys membranes for fungicidal activity.

NO, a biologically active molecule, can diffuse approximately 100 μm under physiological conditions and penetrate cells.[54] To examine the effective cell penetration of NO, DAF-FM DA, an NO fluorescence probe, was used to evaluate the diffusion of NO in fungal cells. Fig. 5e shows the intracellular accumulation of NO. A negligible autofluorescence signal is observed in *C. albicans* suspensions at 0 min. However, after 30 min of exposure to PILMN-NO, a weak green fluorescence signal is emitted, which gradually enhances at 60 min, implying increased intracellular accumulation of NO. The green fluorescence signal gradually weakens at 90 min due to cell membrane damage, inducing NO leakage. Overall, the NO released from PILMN-NO gradually diffuses into fungal cells and is consumed in cells over time to target the DNA and cytoplasm of microbes, causing deamination and oxidative damage to microbial structures and leading to microbe death.[55]

Cytotoxicity and hemolysis assay

Biocompatibility of biomaterials is the prime concern for *in vivo* biomedical applications. Accordingly, the cytocompatibility and hemocompatibility of the prepared MNs were evaluated. The cytotoxicity of the prepared MNs was evaluated by MTT assay against mouse fibroblast cells (L929) and NIH 3T3 cells. Fig. 6a and b show that the cell viability of L929 cells was 83.37% ± 5.47% and 78.03% ± 2.17%, and the cell viability of 3T3 cells was 82.12% ± 1.65% and 79.72% ± 2.31% after PILMN and PILMN-NO treatments, respectively, suggesting no significant cytotoxicity. The cytotoxicity of PILMN-NO is slightly higher than that of PILMN, which may be due to the accumulation of intracellular RNS derived from the released NO, which may cause cellular damage to some extent.

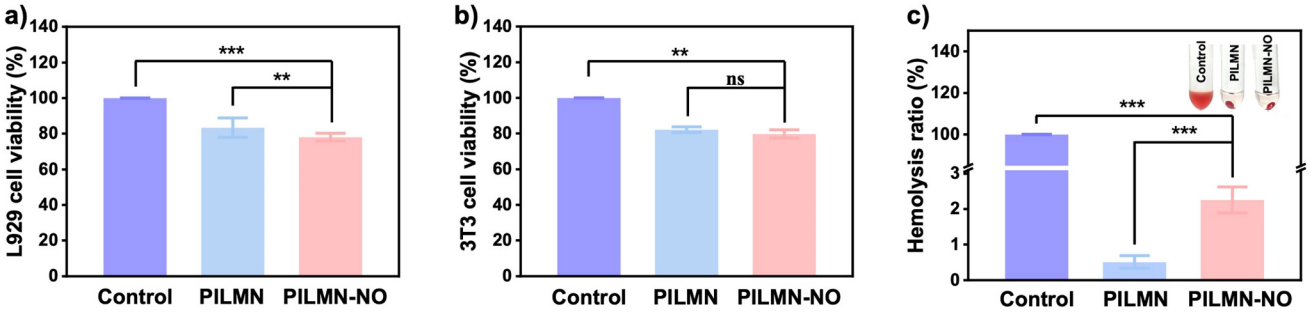

Fig. 6 (a) Cell viability of L929 cells and (b) 3T3 cells after treatment with PILMN and PILMN-NO for 24 h, respectively. Error bars are based on SD (n = 6) (c) Hemolysis ratio of PILMN and PILMN-NO after incubation with red blood cells for 3 h. Error bars are based on SD (n = 6). Note: *p < 0.05, **p < 0.01, and ***p < 0.001.

Published on 07 martie 2023. Downloaded on 05.06.2026 15:08:56.

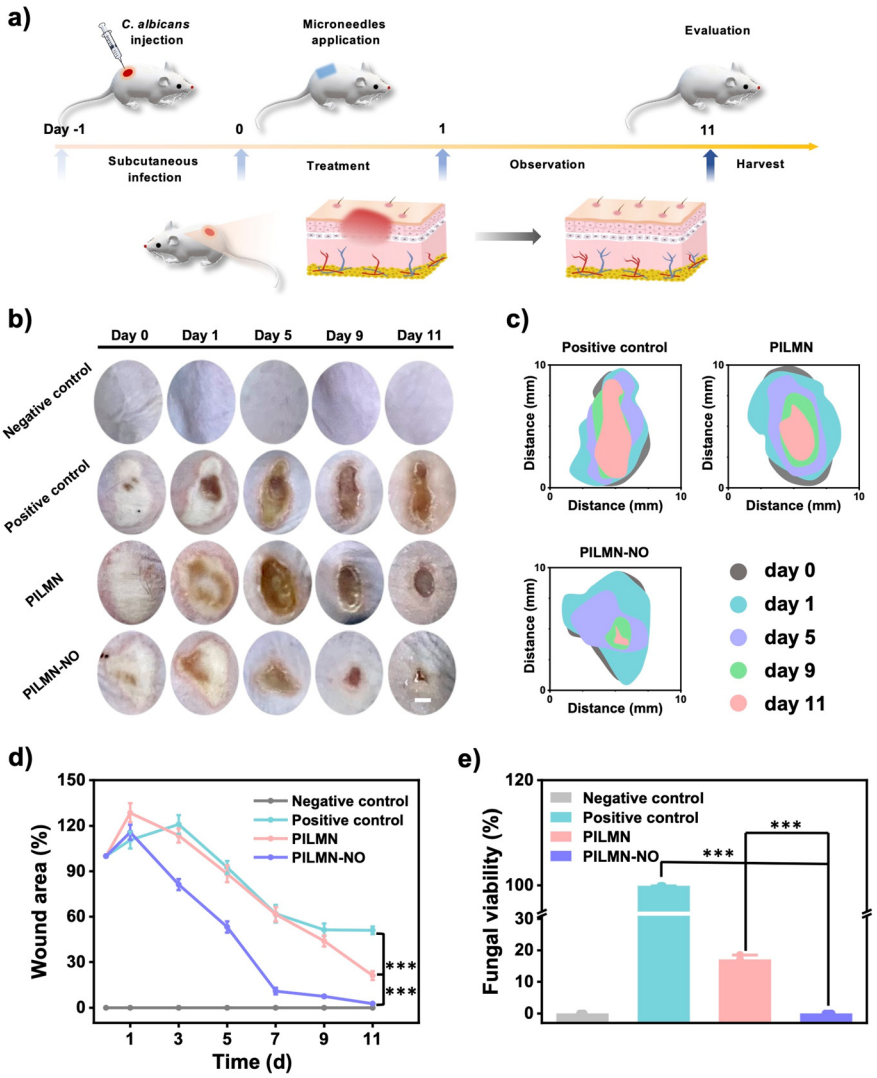

Fig. 7 The performance of the synthesized MNs in the subcutaneous abscess healing process *in vivo*. (a) Schematic illustrating the building model of *C. albicans*-induced subcutaneous abscess and the process of the synthesized MNs treatment *in vivo*. (b) Representative images of the *C. albicans*-infected abscess site in mice at day 0, 1, 5, 9 and 11 (scale bar: 2 mm). (c) Schematic diagram of the wound healing process. (d) Quantitative analysis of the infected areas after receiving different treatments on day 0, 1, 3, 5, 7, 9 and 11. Note: *p < 0.05, **p < 0.01, and ***p < 0.001. (e) Fungal viabilities of *C. albicans* in the abscess site after treatments for 3 days. Note: *p < 0.05, **p < 0.01, and ***p < 0.001.

This journal is © The Royal Society of Chemistry 2023

Published on 07 martie 2023. Downloaded on 05.06.2026 15:08:56.

Hemocompatibility towards red cells is another important index to assess the biocompatibility of biomaterials. The results in Fig. 6c show that the hemolysis ratios are 0.52% ± 0.17% and 2.26% ± 0.59% for PILMN and PILMN-NO, respectively, suggesting that the constructed MNs are compatible with blood cells. All these results indicate the good biocompatibility of the constructed MNs for biomedical applications.

In vivo subcutaneous abscess treatment performance

Inspired by the *in vitro* antifungal and biofilm elimination effects as well as good biocompatibility of the prepared MNs, the *in vivo* antifungal performance of PILMN and PILMN-NO was evaluated in subcutaneous fungal abscess animal models (Fig. 7a). All animal procedures were performed in accordance with the Guidelines for Care and Use of Laboratory Animals of Soochow University and approved by the Animal Ethics Committee of Soochow University.

C. albicans can cause serious deep skin and tissue infections, showing flushing, blistering and even forming subcutaneous fungal abscesses. The subcutaneous fungal abscess mouse model was established by injecting 100 μL of *C. albicans* suspension under epidermis. An obvious subepidermal abscess formed after 1 day, indicating severe fungal infection. The effects of the prepared MNs on the wound healing process were evaluated by estimating the wound closure ratio, fungal viability, H&E staining analysis, collagen deposition and angiogenesis performance. Mice treated with PILMN and PILMN-NO were the test groups. The infected mice without any treatment were used as a positive control, and the mice injected with 100 μL PBS were classified as the negative control. As displayed in Fig. 7b and c, representative images of *C. albicans*-induced subepidermal abscesses on days 0, 1, 5, 9 and 11 are presented. Compared with the positive control group, the abscesses in the PILMN-NO group healed obviously, indicating a better wound healing promotion effect of PILMN-NO. The wound size was quantitatively assessed during the healing process, as illustrated in Fig. 7d. The wound size in the PILMN-NO treated group was significantly reduced and obviously smaller than that in the negative control group, demonstrating that PILMN-NO could effectively treat the subepidermal abscess and promote wound healing by the synergis-

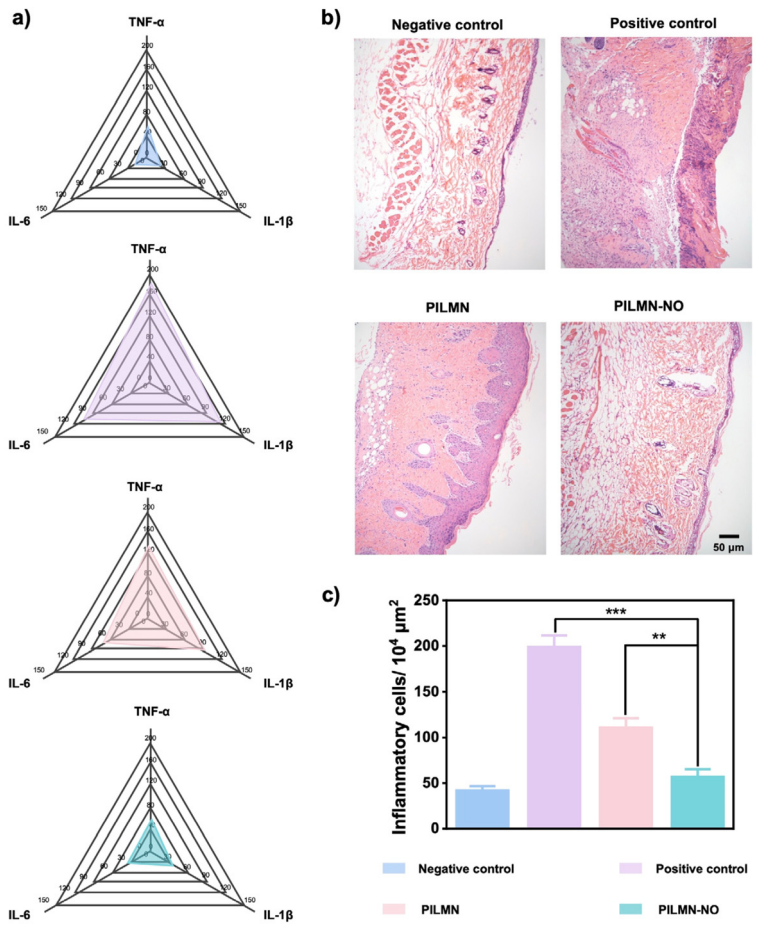

Fig. 8 *In vivo* anti-inflammatory activity of diverse MNs. (a) Expression level (pg mL^{-1}) of TNF-α, IL-6, and IL-1β after different treatments on day 11. (b) H&E staining images of the skin tissue of the abscess site in mice after treatments for 11 days and (c) corresponding statistical analysis of inflammatory cells. Note: *$p < 0.05$, **$p < 0.01$, and ***$p < 0.001$.

Published on 07 martie 2023. Downloaded on 05.06.2026 15:08:56.

tic effect of PIL and the released NO. After being treated for 3 days, the infected tissue sites were collected to quantitate the antifungal activities against *C. albicans* by plate counting method. Compared with the positive control group, the fungal viabilities of the PILMN and PILMN-NO groups were approximately 17.6% and 0%, respectively, suggesting super fungal killing abilities of PILMN-NO *in vivo* (Fig. 7e and Fig. S10†). For open wounds without infection, the wound size in the PILMN-NO treated group was also significantly reduced and obviously smaller than that in the control group (Fig. S11†). Notably, the speed of wound healing accelerated with increasing NO release. These results suggest that PILMN-NO can also promote the healing of noninfected wounds, and the performance of promoting wound healing is positively related to the dosing of NO within a certain range. The wound healing process is usually accompanied by inflammation elimination, collagen deposition, and angiogenesis.[56,57] To further evaluate the biomedical performance of the synthesized MNs for subepidermal abscess treatment, histological and immunohistochemical analyses were performed after subcutaneous injection of *C. albicans* on day 11. The anti-inflammatory response was determined by evaluating tumor necrosis factor-α (TNF-α),

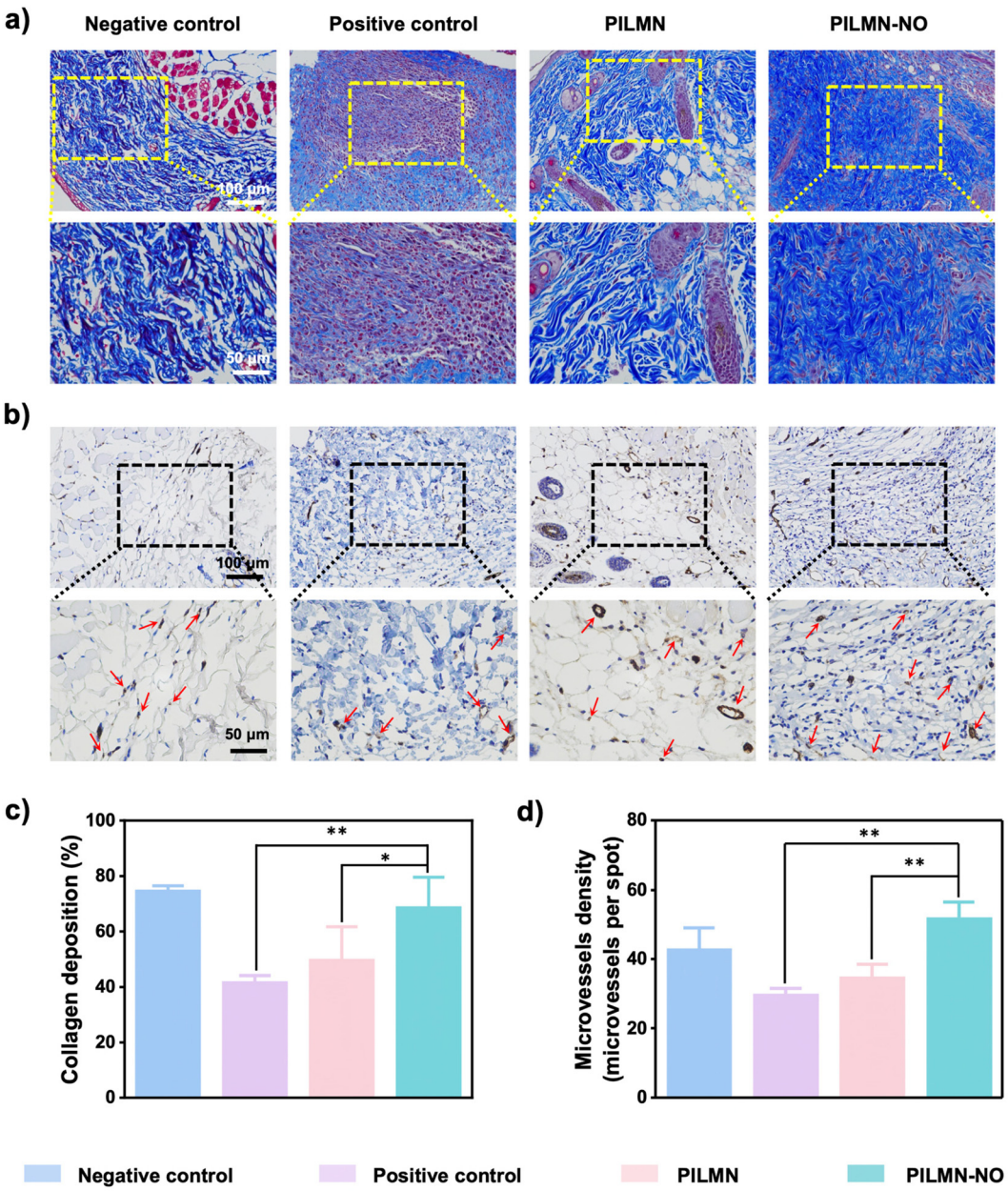

Fig. 9 *In vivo* collagen deposition and angiogenesis activity of diverse MNs. (a) Masson trichrome staining for collagen deposition in tissues (the collagen in the endodermis was stained blue). (b) CD31 immunostaining of different tissues (red arrow: blood vessel) (c) Statistical analysis of collagen deposition. (d) Statistical analysis of microvessels. Note: *$p < 0.05$, **$p < 0.01$, and ***$p < 0.001$.

This journal is © The Royal Society of Chemistry 2023

Published on 07 martie 2023. Downloaded on 05.06.2026 15:08:56.

interleukin-1 (IL-1β), and interleukin-6 (IL-6) with enzyme-linked immunosorbent assay (ELISA). Fig. 8a shows that the inflammatory factors significantly decreased in mice treated with PILMN and PILMN-NO compared with the positive control group. In particular, the inflammatory response of the PILMN-NO treated mice was similar to that of the negative control group. This was consistent with the healing results, indicating the anti-inflammatory effects of PILMN-NO in the subepidermal abscess infection model. Similar results were also obtained in noninfected open wounds. Fig. S12† shows that the expression of the abovementioned inflammatory factors significantly decreased in the mice treated with PILMN-NO compared with the control group, and increasing NO release led to a reduction in the inflammatory response. These results show that the released NO effectively downregulated the inflammatory responses. Subsequently, H&E staining of the *C. albicans*-infected skin tissues was performed. Fig. 8b shows the formation of new granulation tissues and epidermis in the PILMN-NO group on day 11, similar to the negative control group. In contrast, few granulation tissues were observed in the positive control group, and loosened tissues and epidermis were observed in the PILMN group. Additionally, large numbers of inflammatory cells appeared in the positive control group, while there were fewer inflammatory cells in the PILMN group. For the PILMN-NO issues, almost no increase in inflammatory cells was observed compared to the negative group, suggesting an effective and potent anti-inflammatory effect of PILMN-NO (Fig. 8c). Collagen deposition plays an important role in the wound healing process, which was investigated using Masson's trichrome staining. Collagen appears blue, while myofibrils appear red. As shown in Fig. 9a and c, compared to the positive control group, significant collagen formation and deposition were observed in the PILMN and PILMN-NO treated groups, especially in the PILMN-NO-treated mice, and collagen formation and deposition were obvious, suggesting promoted wound healing activity. Immunohistochemical staining of CD31 was performed to study the neovascularization of skin (Fig. 9b and d). The CD31 images revealed markedly increased densities of microvessels in the PILMN-NO group compared with the negative control group, suggesting an acceleration of wound healing by promoting microvessels and alleviating local hypoxia. All these results demonstrate that PILMN-NO can effectively promote wound healing through anti-inflammation, collagen deposition, and angiogenesis effects by releasing and delivering NO to the subcutaneous tissue.

3. Conclusions

In summary, multifunctional NO-releasing imidazolium-type PIL-based MN patches (PILMN-NO) were developed for the treatment of subcutaneous fungal infections with the following *in vivo* features: (i) transdermal delivery and precise and sustained release of NO to the infection site by MN, (ii) superior antifungal properties and biofilm ablation ability due to the synergistic membrane-disruption mechanism effect of PIL and released NO, (iii) facilitated anti-inflammation, collagen deposition, and angiogenesis abilities, and (iv) significant acceleration of wound healing performance with two hours of treatment. Significantly, the therapeutic strategy provides an efficient microbicidal strategy, addressing the permeation and targeting challenge of administration and making a breakthrough in the field of subcutaneous infection in the postantibiotic era. PIL and NO integrated with an MN delivery system could be promising candidates for subcutaneous infection and exert wide application prospects in related biomedical fields.

Data availability

The datasets supporting this article have been uploaded as part of this manuscript and its corresponding ESI.†

Author contributions

F. Y. and J. G. conceived and designed the project. Q. Z. synthesized and fully characterized all materials. Z. Z. and H. X. completed the animal experiment together. X. Z. completed quantum chemical calculations. Z. L. and Q. L. assisted with data analysis. S. G. provided some starting materials. F. Y., J. G. and Q. Z. drafted the manuscript. All authors have discussed the results and given approval to the manuscript.

Conflicts of interest

The authors declare no conflict of interest.

Acknowledgements

This work was supported by the National Natural Science Foundation of China (No. 21835005, U1862109), Science and Technology Development Plan Project of Suzhou (SNG2021011), Livelihood Technology Project of Suzhou (SKJY2021042), Collaborative Innovation Center of Suzhou Nano Science and Technology, the Project Funded by the Priority Academic Program Development of Jiangsu Higher Education Institutions.

References

1 D. Simões, S. P. Miguel, M. P. Ribeiro, P. Coutinho, A. G. Mendonça and I. J. Correia, *Eur. J. Pharm. Biopharm.*, 2018, **127**, 130–141.
2 K. T. Clebak and M. A. Malone, *Primary Care: Clin. Off. Pract.*, 2018, **45**, 433–454.

Published on 07 martie 2023. Downloaded on 05.06.2026 15:08:56.

3 A. F. Cardona and S. E. Wilson, *Clin. Infect. Dis.*, 2015, **61**, S69–S78.
4 J. P. Burnham, J. P. Kirby and M. H. Kollef, *Intensive Care Med.*, 2016, **42**, 1899–1911.
5 G. D. Brown, D. W. Denning, N. A. R. Gow, S. M. Levitz, M. G. Netea and T. C. White, *Sci. Transl. Med.*, 2012, **4**, 165rv13.
6 A. Puel, *Hum. Genet.*, 2020, **139**, 1011–1022.
7 R. Jamaledin, C. K. Y. Yiu, E. N. Zare, L. N. Niu, R. Vecchione, G. Chen, Z. Gu and F. R. Tay, *Adv. Mater.*, 2020, **32**, 2002129.
8 B. S. Li, J. H. Cary and H. I. Maibach, *Arch. Dermatol. Res.*, 2018, **310**, 537–549.
9 F. Bongomin, S. Gago, R. O. Oladele and D. W. Denning, *J. Fungi*, 2017, **3**, 57.
10 W. Jiang, M. Zhou, Z. Cong, J. Xie, W. Zhang, S. Chen, J. Zou, Z. Ji, N. Shao, X. Chen, M. Li and R. Liu, *Angew. Chem., Int. Ed.*, 2022, **61**, e202200778.
11 J. R. Perfect, *Nat. Rev. Drug Discovery*, 2017, **16**, 603–616.
12 D. A. Riccio and M. H. Schoenfisch, *Chem. Soc. Rev.*, 2012, **41**, 3731–3741.
13 R. Namivandi-Zangeneh, E. H. H. Wong and C. Boyer, *ACS Infect. Dis.*, 2021, **7**, 215–253.
14 M. Chen, J. Zhou, P. Ran, F. Lei, J. Meng, J. Wei and X. Li, *Adv. Healthcare Mater.*, 2022, 2200199.
15 N. Stasko, K. McHale, S. J. Hollenbach, M. Martin and R. Doxey, *Antimicrob. Agents Chemother.*, 2018, **62**, e01026–e01017.
16 F. Madariaga-Venegas, R. Fernández-Soto, L. F. Duarte, N. Suarez, D. Delgadillo, J. A. Jara, R. Fernández-Ramires and B. Urzia, *PLoS One*, 2017, **12**, e0176755.
17 L. D. Blackman, Y. Qu, P. Cass and K. E. S. Locock, *Chem. Soc. Rev.*, 2021, **50**, 1587–1616.
18 A. M. Garzón-Porras, D. L. Bertuzzi, K. Lucas, L. C. E. da Silva, M. G. de Oliveira and C. Ornelas, *ACS Appl. Polym. Mater.*, 2020, **2**, 2027–2034.
19 A. Liu, Q. Wang, Z. Zhao, R. Wu, M. Wang, J. Li, K. Sun, Z. Sun, Z. Lv, J. Xu, H. Jiang, M. Wan, D. Shi and C. Mao, *ACS Nano*, 2021, **15**, 13339–13350.
20 S. Yao, Y. Wang, J. Chi, Y. Yu, Y. Zhao, Y. Luo and Y. Wang, *Adv. Sci.*, 2022, **9**, 2103449.
21 L. Yang, E. S. Feura, M. J. R. Ahonen and M. H. Schoenfisch, *Adv. Healthcare Mater.*, 2018, **7**, 1800155.
22 X. Lv, K. Chen, G. Shi, W. Lin, H. Bai, H. Li, G. Tang and C. Wang, *Sci. Adv.*, 2020, **6**, eabb7788.
23 N. Cao, L. Gan, Q. Xiao, X. Lv, W. Lin, H. Li and C. Wang, *ACS Sustainable Chem. Eng.*, 2020, **8**, 2990–2995.
24 Y. Sun, S. Ren, Y. Hou, K. Zhang, Q. Zhang and W. Wu, *ACS Sustainable Chem. Eng.*, 2020, **8**, 3283–3290.
25 M. Wang, J. Shi, H. Mao, Z. Sun, S. Guo, J. Guo and F. Yan, *Biomacromolecules*, 2019, **20**, 3161–3170.
26 D. Bedrov, J. P. Piquemal, O. Borodin, A. D. MacKerell, B. Roux and C. Schröder, *Chem. Rev.*, 2019, **119**, 7940–7995.
27 L. Ma, C. J. E. Haynes, A. B. Grommet, A. Walczak, C. C. Parkins, C. M. Doherty, L. Longley, A. Tron, A. R. Stefankiewicz, T. D. Bennett and J. R. Nitschke, *Nat. Chem.*, 2020, **12**, 270–275.
28 J. M. Gomes, S. S. Silva and R. L. Reis, *Chem. Soc. Rev.*, 2019, **48**, 4317–4335.
29 P. Halder, S. Kundu, S. Patel, A. Setiawan, R. Atkin, R. Parthasarthy, J. Paz-Ferreiro, A. Surapaneni and K. Shah, *Renew. Sustain. Energy Rev.*, 2019, **105**, 268–292.
30 J. Guo, Q. Xu, Z. Zheng, S. Zhou, H. Mao, B. Wang and F. Yan, *ACS Macro Lett.*, 2015, **4**, 1094–1098.
31 J. Yang, Y. Li, R. Ye, Y. Zheng, X. Li, Y. Chen, X. Xie and L. Jiang, *Microsyst. Nanoeng.*, 2020, **6**, 112.
32 R. F. Donnelly, R. Majithiya, T. R. R. Singh, D. I. J. Morrow, M. J. Garland, Y. K. Demir, K. Migalska, E. Ryan, D. Gillen, C. J. Scott and A. D. Woolfson, *Pharm. Res.*, 2011, **28**, 41–57.
33 T. Zhang, B. Sun, J. Guo, M. Wang, H. Cui, H. Mao, B. Wang and F. Yan, *Acta Biomater.*, 2020, **115**, 136–147.
34 G. K. Mani, K. Miyakoda, A. Saito, Y. Yasoda, K. Kajiwara, M. Kimura and K. Tsuchiya, *ACS Appl. Mater. Interfaces*, 2017, **9**, 21651–21659.
35 H. Lee, T. K. Choi, Y. B. Lee, H. R. Cho, R. Ghaffari, L. Wang, H. J. Choi, T. D. Chung, N. Lu, T. Hyeon, S. H. Choi and D. H. Kim, *Nat. Nanotechnol.*, 2016, **11**, 566–572.
36 S. P. Davis, W. Martanto, M. G. Allen and M. R. Prausnitz, *IEEE Trans. Biomed. Eng.*, 2005, **52**, 909–915.
37 X. Zhang, X. Fu, G. Chen, Y. Wang and Y. Zhao, *Adv. Sci.*, 2021, **8**, 2101210.
38 J. Xu, R. Danehy, H. Cai, Z. Ao, M. Pu, A. Nusawardhana, D. Rowe-Magnus and F. Guo, *ACS Appl. Mater. Interfaces*, 2019, **11**, 14640–14646.
39 Y. Su, V. L. Mainardi, H. Wang, A. McCarthy, Y. S. Zhang, S. Chen, J. V. John, S. L. Wong, R. R. Hollins, G. Wang and J. Xie, *ACS Nano*, 2020, **14**, 11775–11786.
40 M. Yin, J. Wu, M. Deng, P. Wang, G. Ji, M. Wang, C. Zhou, N. T. Blum, W. Zhang, H. Shi, N. Jia, X. Wang and P. Huang, *ACS Nano*, 2021, **15**, 17842–17853.
41 J. Yu, J. Wang, Y. Zhang, G. Chen, W. Mao, Y. Ye, A. R. Kahkoska, J. B. Buse, R. Langer and Z. Gu, *Nat. Biomed. Eng.*, 2020, **4**, 499–506.
42 H. P. Tham, K. Xu, W. Q. Lim, H. Chen, M. Zheng, T. G. S. Thng, S. S. Venkatraman, C. Xu and Y. Zhao, *ACS Nano*, 2018, **12**, 11936–11948.
43 K. Chen, G. Shi, X. Zhou, H. Li and C. Wang, *Angew. Chem., Int. Ed.*, 2016, **55**, 14364–14368.
44 X. Pan, G. Quan, C. Wu, M. Chen, D. Yang, Y. Sun, T. Liu, W. Wang, J. Fu, Q. Wang and X. Bai, *ACS Nano*, 2021, **15**, 3387–3401.
45 G. K. K. Reddy and Y. V. Nancharaiah, *Front. Microbiol.*, 2020, **11**, 730.
46 E. M. Hetrick, J. H. Shin, N. A. Stasko, C. B. Johnson, D. A. Wespe, E. Holmuhamedov and M. H. Schoenfisch, *ACS Nano*, 2008, **2**, 235–246.
47 P. C. Naha, Y. Liu, G. Hwang, Y. Huang, S. Gubara, V. Jonnakuti, A. Simon-Soro, D. Kim, L. Gao, H. Koo and D. P. Cormode, *ACS Nano*, 2019, **13**, 4960–4971.
48 J. Duan and D. L. Kasper, *Glycobiology*, 2011, **21**, 401–409.
49 J. Wang, L. Wang, J. Pan, J. Zhao, J. Tang, D. Jiang, P. Hu, W. Jia and J. Shi, *Adv. Sci.*, 2021, **8**, 2004010.

 This journal is © The Royal Society of Chemistry 2023

50 P. Zhang, S. Li, H. Chen, X. Wang, L. Liu, F. Lv and S. Wang, *ACS Appl. Mater. Interfaces*, 2017, **9**, 16933–16938.
51 H. S. Schrekker, R. K. Donato, A. M. Fuentefria, V. Bergamo, L. F. Oliveira and M. M. MacHado, *MedChemComm*, 2013, **4**, 1457–1460.
52 J. Zhu, J. Tian, C. Yang, J. Chen, L. Wu, M. Fan and X. Cai, *Small*, 2021, **17**, 2101495.
53 R. Garcia-Rubio, H. C. de Oliveira, J. Rivera and N. Trevijano-Contador, *Front. Microbiol.*, 2020, **10**, 2993.
54 H. Jeong, D. Choi, Y. Oh, J. Heo and J. Hong, *Adv. Healthcare Mater.*, 2021, **11**, 2102095.
55 Y. Lu, D. L. Slomberg, A. Shah and M. H. Schoenfisch, *Biomacromolecules*, 2013, **14**, 3589–3598.
56 Y. Oh, H. Jeong, S. Lim and J. Hong, *Biomacromolecules*, 2020, **21**, 4972–4979.
57 C. H. Su, W. P. Li, L. C. Tsao, L. C. Wang, Y. P. Hsu, W. J. Wang, M. C. Liao, C. L. Lee and C. S. Yeh, *ACS Nano*, 2019, **13**, 4290–4301.

Published on 07 martie 2023. Downloaded on 05.06.2026 15:08:56.